In-Plane Magnetic Anisotropy of Fe Atoms on Bi$_2$Se$_3$(111)

J. Honolka,[1,*] A. A. Khajetoorians,[2,†] V. Sessi,[3] T. O. Wehling,[4,5,6] S. Stepanow,[1] J.-L. Mi,[7] B. B. Iversen,[7] T. Schlenk,[2]
J. Wiebe,[2] N. B. Brookes,[3] A. I. Lichtenstein,[4] Ph. Hofmann,[8] K. Kern,[1,9] and R. Wiesendanger[2]

[1]*Max-Planck-Institut für Festkörperforschung, Heisenbergstrasse 1, 70569 Stuttgart, Germany*
[2]*Institute for Applied Physics, Universität Hamburg, D-20355 Hamburg, Germany*
[3]*European Synchrotron Radiation Facility, BP 220, F-38043 Grenoble, France*
[4]*I. Institut für Theoretische Physik, Universität Hamburg, D-20355 Hamburg, Germany*
[5]*Institut für Theoretische Physik, Universität Bremen, Otto-Hahn-Allee 1, D-28359 Bremen, Germany*
[6]*Bremen Center for Computational Materials Science, Universität Bremen, Am Fallturm 1a, D-28359 Bremen, Germany*
[7]*Center for Materials Crystallography, Department of Chemistry, Interdisciplinary Nanoscience Center,
Aarhus University, 8000 Aarhus C, Denmark*
[8]*Department of Physics and Astronomy, Interdisciplinary Nanoscience Center, Aarhus University, 8000 Aarhus C, Denmark*
[9]*Institut de Physique de la Matière Condensée, Ecole Polytechnique Fédérale de Lausanne, CH-1015 Lausanne, Switzerland*
(Received 20 December 2011; published 22 June 2012)

The robustness of the gapless topological surface state hosted by a 3D topological insulator against perturbations of magnetic origin has been the focus of recent investigations. We present a comprehensive study of the magnetic properties of Fe impurities on the prototypical 3D topological insulator Bi$_2$Se$_3$ using local low-temperature scanning tunneling spectroscopy and integral x-ray magnetic circular dichroism techniques. Single Fe adatoms on the Bi$_2$Se$_3$ surface, in the coverage range $\approx 1\%$ of a monolayer, are heavily relaxed into the surface and exhibit a magnetic easy axis within the surface plane, contrary to what was assumed in recent investigations on the supposed opening of a gap. Using *ab initio* approaches, we demonstrate that an in-plane easy axis arises from the combination of the crystal field and dynamic hybridization effects.

Topological insulators (TIs) have demanded heavy interest from the scientific community as a new class of materials illuminating fascinating yet exotic physics and offering large potential for applications in the field of spintronics [1]. TIs host a gapless topological surface state (TSS) which exhibits a Dirac-cone-like dispersion. However, unlike in the case of graphene, the Dirac cone is located in the center of the Brillouin zone and the spin and momentum degrees of freedom are locked. The latter so-called topological quality of the TSS is protected by time-reversal symmetry, which leads to a variety of interesting effects [2–4].

The locking of both spin and momentum degrees of freedom leads to the suppression of the 180° elastic backscattering of TSS electrons in the absence of spin-flip processes. The robustness of these ''topologically protected'' processes, when introducing impurities which break time-reversal symmetry, is of critical importance for spin-based transport in such materials. It has been suggested that the interaction between magnetic impurities and the TSS can cause an opening of an energy gap at the Dirac point (DP), provided that the magnetic order is oriented normal to the surface plane [5–7]. Nevertheless, the stability of the TSS against local magnetic perturbations is currently under heavy debate [8–10], since a characterization of the magnetic properties of surface adsorbates such as Fe or Co [11] is still sparse.

In this Letter, we present a comprehensive study of the magnetic properties of Fe impurities on Bi$_2$Se$_3$, a prototypical TI, using local scanning tunneling microscopy (STM) and integral x-ray magnetic circular dichroism (XMCD) techniques. We show that the multiplet structure visible in x-ray absorption spectra reflects the high-spin state of single Fe atoms which adsorb at hollow sites of the surface lattice and are influenced by the resultant trigonal crystal fields. XMCD reveals that these Fe atoms have an in-plane magnetic easy axis resulting from significant magnetic anisotropy. This observation is supported by our density functional theory calculations, which reveal the possibility of a preferred in-plane easy axis when considering both crystal field and dynamic hybridization effects.

Both local scanning tunneling spectroscopy and integral XMCD measurements were carried out with one and the same Bi$_2$Se$_3$ crystal used in Ref. [10]. Clean Bi$_2$Se$_3$(111) surfaces were obtained by *in situ* cleaving at room temperature under ultrahigh vacuum conditions followed by a fast cooldown to temperatures of about $T = 10$ K within 15 minutes. In order to prevent surface diffusion, Fe was deposited at low temperatures, ≈ 10 K, onto Bi$_2$Se$_3$(111), using an *e*-beam evaporator for both experiments. For the case of x-ray measurements, the general procedure of *in situ* metal atom deposition and coverage calibration is described in detail in Ref. [12]. Measurements were carried out at the ID08 beam line of the ESRF in Grenoble.

Scanning tunneling spectroscopy was performed at a temperature of $T = 0.3$ K using a home-built ultrahigh vacuum STM with a tungsten tip [13]. Figure 1(a) shows a constant-current image of $\approx 1\%$ of a monolayer (ML) Fe deposited on a clean Bi_2Se_3 surface. Single Fe atoms are observed at two different hollow sites with respect to the underlying Se lattice, with nearly equal probability. High-resolution images [Fig. 1(b)] show that the atoms on the two binding sites, labeled A and B, clearly differ in apparent height and shape. The apparent heights of 0.5 and 0.3 Å for A and B, respectively, are small compared to, e.g., Fe atoms on Cu(111) (≈ 1 Å, [14]), and remain nearly constant over a large range of bias voltages (-0.4 to 1 V). A closer inspection reveals that the apparent shape of the Fe and the halo (charge density) surrounding the atom depends on the binding site. Type A atoms show a circular protrusion around the center of the Fe atom, while type B atoms show a triangular protrusion. The halo pattern is quite complex but unique for each binding site. Infrequent hopping events of a single Fe atom between A and B stacking positions indicate a transformation of atom shape and halo between the two distinguishable atom types and binding sites. These latter properties are purely electronic effects resulting from the bonding between the Fe atom and the atomically flat Bi_2Se_3 surface.

Tunneling spectra [$dI/dV(V)$] that were taken on the bare Bi_2Se_3 surface prior to Fe deposition [Fig. 1(c) (black line)] exhibit a minimum in an energy window around
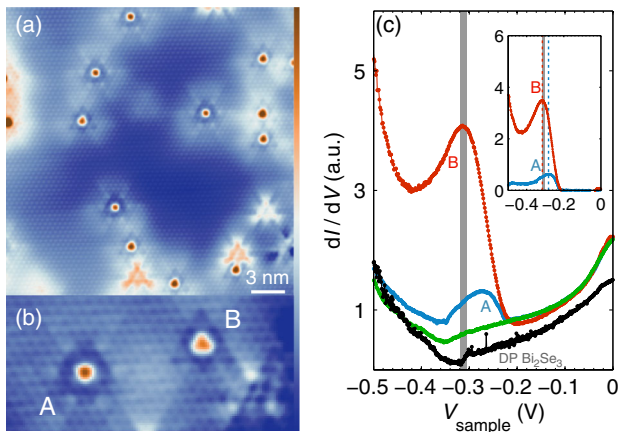

FIG. 1 (color online). (a) STM constant-current image of 1% ML of Fe atoms adsorbed onto a cleaved Bi_2Se_3 surface; $I_{stab} = 500$ pA and $V_{stab} = +100$ mV. (b) High-resolution image of two Fe atoms at different binding sites (A and B); $I_{stab} = 600$ pA and $V_{stab} = -100$ mV. (c) Tunneling spectra taken on two Fe atoms at the indicated binding sites and on a substrate spot [green (gray) line] of the Fe covered surface. For reference, a spectrum on the uncovered Bi_2Se_3 surface is shown (black line), where the thick vertical gray bar refers to the DP, as confirmed by probing the zeroth Landau level in high magnetic fields. Inset: same as (c) after subtracting the substrate spectrum; $I_{stab} = 600$ pA, $V_{stab} = -100$ mV, $V_{mod} = 3$ mV, and $f_{mod} = 4.1$ kHz.

-0.31 eV (thick vertical gray bar). Spectra in different magnetic fields perpendicular to the surface (not shown) prove that this minimum coincides with the zeroth Landau level of the TSS and thus with the location of the DP of the bare Bi_2Se_3 [15,16]. This is consistent with angle-resolved photoemission spectroscopy (ARPES) measurements of the band structure of the same crystal [10] and typical for naturally grown Bi_2Se_3 crystals, which are known to be electron-doped due to the presence of Se vacancies observable in STM images [Fig. 1(a)] [17,18]. Upon deposition of Fe [Fig. 1(c) (green [gray] line)], the minimum shifts downwards with respect to the impurity-free surface by about 50 meV when compared to the DP of the impurity-free surface. We conclude that Fe acts as a donor, and the DP is accordingly shifted downwards, in contradiction to recent ARPES measurements [9]. However, there are no indications of a gap near the DP after Fe adsorption. Instead, a resonance can be seen in spectra taken on the Fe atoms. It appears at voltages slightly above the DP and has differing intensities, peak positions, and linewidths, depending on the binding site. Substrate-corrected spectra (inset) prove that the resonance has a considerably stronger intensity and is shifted closer to the DP for the type B Fe atoms. Similar resonances have been observed on the Se vacancies [17,18] and were attributed to Coulomb scattering of the topological surface state by the impurity [8,18].

For a magnetic characterization, x-ray absorption spectra (XAS) at the Fe $L_{3,2}$ absorption edges (708.0 and 721.0 eV, respectively) were recorded in the total electron yield mode for different angles θ between the Bi_2Se_3 surface normal and the x-ray beam direction. Magnetic fields B were applied collinear to the beam, as shown in the inset of Fig. 2(a). The experimental time scales for measuring spectra are on the order of 100 s. Before and after the magnetic characterization, the samples were carefully checked for oxygen contaminations using the XAS at the O-1s absorption edge.

Typical nondichroic XAS, defined as the average of XAS for right (σ^+) and left (σ^-) circular polarization, are shown after Bi_2Se_3 background subtraction in the upper panels of Figs. 2(c) and 2(d). When B is applied, a pronounced XMCD signal defined as ($\sigma^+ - \sigma^-$) is observed, which reflects the spin and orbital polarization in the Fe 3d states. As a first approximation, the XMCD signal is proportional to the average Fe magnetization M when it is normalized to the L_3 peak intensity in the XAS signal, as shown in the lower panels of Figs. 2(c) and 2(d) for fields of $B = 5$ T. More precisely, the XMCD signal normalized to the total XAS intensity is proportional to the projection of the averaged Fe moments $\langle \vec{m} \rangle$ on the photon propagation direction $\vec{\Sigma}$. Comparing the lower panels of Figs. 2(c) and 2(d), we thus conclude that Fe atoms prefer to be magnetized in the $\theta = 70°$ (in-plane) direction, as compared to the out-of-plane case where $\theta = 0°$.
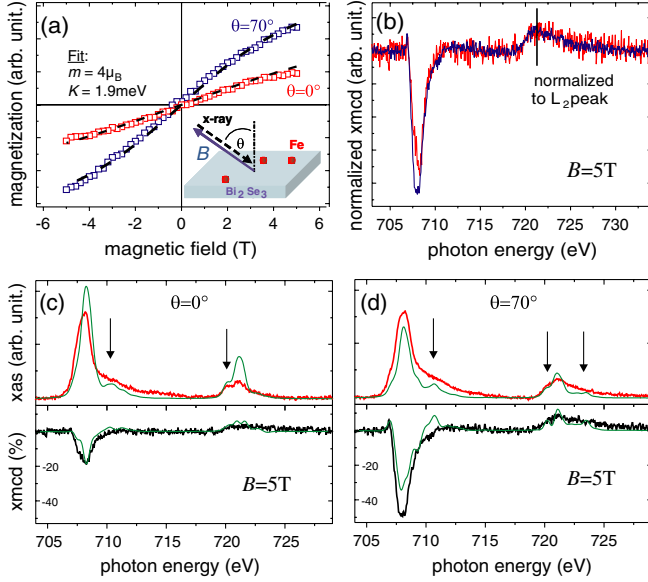
FIG. 2 (color online). X-ray study of Fe impurities (coverage 1% ML) on Bi_2Se_3 at $T = 10$ K. (a) Magnetization curves $M(B)$ for directions $\theta = 0°$, $70°$ in red (gray) and blue (black) squares, respectively. The dashed lines represent thermodynamic fits with a moment $m = 4 \mu_B$ and $K = 1.9$ meV (see text). (b) XMCD signals in a field of $B = 5$ T normalized to the XMCD peak intensity at the L_2 edge. (c),(d) XAS [red (dark gray) line, upper panel] and XMCD (black line, lower panel) measured in a field of $B = 5$ T for directions (c) $\theta = 0°$ and (d) $70°$. Green (light gray) spectra refer to CF calculations with $\epsilon_0 = -0.69$ eV and $\epsilon_2 = 0.32$ eV.

This is supported by the significant anisotropy in the orbital moment m_L visible in Fig. 2(b): the XMCD spectra are normalized to their peak intensity at the L_2 edge, and smaller intensities at the L_3 edge for $\theta = 0°$ [red (gray) curve] indicate considerably reduced orbital moments m_L with respect to $\theta = 70°$ [blue (black) curve]. By measuring the normalized XMCD intensity at the L_3 edge for different magnetic fields, it is possible to obtain magnetization curves $M(B)$. The curves $M(B)$ in Fig. 2(a) at $\theta = 0°$, $70°$ show smaller values along $\theta = 0°$, again proving a preferential orientation of the magnetization in the surface plane.

In order to quantify the observed magnetic properties, we analyze the spectra using crystal field (CF) multiplet calculations, including electron repulsion and spin-orbit coupling [19]. The XAS line shape in Figs. 2(c) and 2(d) reflects the electronic configuration and possible CF effects from the Bi_2Se_3 surface. A pronounced double-peak structure is observed at the L_2 edge as well as a shoulder at the high-energy side of the L_3 edge (see arrows). The CF multiplet calculations can reproduce these main features, assuming a purely trigonal CF of C_{3v} symmetry. In this environment, the Fe d orbitals decompose into two twofold degenerate blocks transforming according to the E-irreducible representation of C_{3v} [we label the

sub-blocks as E_1 (d_{xz}, d_{yz}) and E_2 ($d_{x^2-y^2}$, d_{xy})] and the d_{z^2} orbital transforming according to the A_1 representation. The CF is then defined through the single-particle on-site energy shifts $\epsilon_0 = \epsilon_{d_{z^2}} - \epsilon_{d_{xz},d_{yz}}$ of the A_1 and $\epsilon_2 = \epsilon_{d_{xy},d_{x^2-y^2}} - \epsilon_{d_{xz},d_{yz}}$ of the E_2 Fe $3d$ orbitals relative to the E_1 orbitals. The green (light gray) curves in Figs. 2(c) and 2(d) represent spectra derived for Fe d^6 impurities in a CF using the parameters $\epsilon_0 = -0.69$ eV and $\epsilon_2 = 0.32$ eV. The double-peak structure in the XAS of the L_2 edge at $\theta = 0°$ as well as the shoulder at the L_3 edge for both $\theta = 0°$ and $70°$ are reproduced. The measured spectra are broadened with respect to the model, which points towards a significant coupling of d states to delocalized bands. From our CF calculations, which also consider Boltzmann statistics at $T = 10$ K, we derive orbital moments with an anisotropic difference of $\Delta m_L = 0.13 \mu_B$ between the two measured geometries supporting the experimentally observed quenching of the orbital moments in the $\theta = 0°$ direction under the influence of the in-plane CFs. Assuming a moment of $|\vec{m}| = 4 \mu_B$, we can fit the experimental magnetization curves in Fig. 2(a) with a thermodynamic model which includes the Zeeman term and an anisotropy term $E_A = K \cdot (\vec{z} \cdot \vec{m}/|m|)^2$, where K is the magnetic anisotropy per Fe atom and $\vec{z}$ the normal of the (111) plane. The fit leads to a significant in-plane magnetic anisotropy of $K = +1.9$ meV per atom. These experimental results are valid as long as the distribution of Fe consists predominantly of single atoms on the surface. At higher coverages ($> 10\%$), STM shows the emergence of variable-size Fe clusters and this coincides with the disappearance of the atomic multiplet features in XAS spectra.

To understand the physical mechanisms behind the experimentally observed magnetic properties of the system, we resort to *ab initio* calculations and derive a quantum impurity model describing the Fe adatoms on the Bi_2Se_3 surface. We performed density functional theory calculations of Fe adatoms on the Bi_2Se_3 surface which yield the relaxed adsorption geometries, the magnetic moments, and the hybridization functions [20–22].

Our calculations reveal two possible adsorption sites for an Fe adatom at an fcc hollow (f) or an hcp hollow (h) site [Figs. 3(a) and 3(b)]. While both adsorption geometries are stable, we find that the f site adsorption yields 0.07 eV lower total energy than the h site. Independent of the adsorption site, the generalized gradient approximation predicts a Fe $3d$ occupancy of $N_d = 6.3$. At both sites, we find a strong relaxation of the adatom into the surface, with equilibrium positions of the Fe adatom virtually at the same height (± 0.1 Å) as the surrounding Se atoms. This is well in line with the STM topography and the observed broadening in the x-ray absorption spectra. It has important consequences for the electronic and magnetic properties of the Fe adatoms.

The energy-dependent coupling strength of the impurity $3d$ orbitals and the surrounding crystal is quantified by the
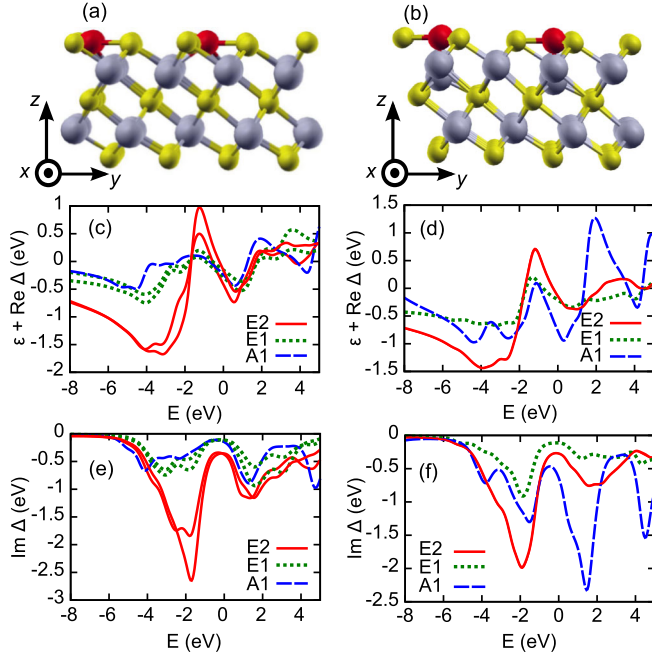
FIG. 3 (color online).   (a),(b) Adsorption geometries of Fe [red (dark gray) spheres] on Bi_2Se_3 [Bi, big light gray spheres; Se, small yellow (light gray) spheres]. Fe can adsorb at (a) an fcc (f site) or (b) an hcp (h site) hollow site. The corresponding real and imaginary parts of the hybridization functions [$Re\Delta_{ii}(E) + \epsilon_i$ and $Im\Delta_{ii}(E)$] are given in (c),(d) and (e),(f), respectively, and quantify the interaction of the Fe $3d$ electrons with their environment. $\Delta_{ii}(E)$ is shown for all Fe $3d$ orbitals: $E2$ (d_{xy} and $d_{x^2-y^2}$), $E1$ (d_{xz} and d_{yz}), and $A1$ (d_{z^2}).

hybridization functions $\Delta_{ij}(E)$, where $i, j = (m, \sigma)$ denote combined orbital and spin quantum numbers of the Fe $3d$ electrons and E is the energy [27]. These hybridization functions can be interpreted as energy-dependent complex valued potentials acting on the Fe $3d$ orbitals and fully characterize their interaction with the substrate as regards local observables (see Refs. [27,28]). For an Fe atom in the h site position [Fig. 3(f)], we find the most pronounced peaks in $Im\Delta_{ii}(E)$ for the in-plane d orbitals (d_{xy} and $d_{x^2-y^2}$ spanning the E_2 subspace of orbital angular momentum quantum number $|l_z| = 2$) at $E \approx -2$ eV and for the out-of-plane oriented d_{z^2} orbital above the Fermi level. For Fe at the energetically most favorable f site [Fig. 3(e)], $Im\Delta_{ii}(E)$ is clearly dominated by peaks at $E \approx -2$ eV in the d_{xy} and $d_{x^2-y^2}$ orbitals. The hybridization of the d_{z^2} orbital is smaller than at the h site because there is no Bi atom directly beneath the Fe atom. Consequently, at both adsorption sites, the in-plane oriented d_{xy} and $d_{x^2-y^2}$ orbitals hybridize strongly with electronic states from the surrounding crystal. The relaxation of the Fe adatoms into the Bi_2Se_3 surface facilitates the strength of this particular hybridization channel.

In order to clarify the consequence of this hybridization on the easy axis, we focus on the population of these orbitals. $Re\Delta_{ii}(E) + \epsilon_i$, with $\epsilon_i = \epsilon_{d_{xy}}, \epsilon_{d_{xz}}, \epsilon_{d_{z^2}}, \ldots$ being the on-site energies of the Fe $3d$ orbitals, can be interpreted as the energy-dependent crystal field, which controls the occupation of the impurity orbitals. Fe has $N_d \sim 6$ d electrons, five of which occupy the spin-up d orbitals. The remaining spin-down d electron determines the magnetic easy axis [27]. If it occupies an orbital with $|l_z| > 0$, one obtains an out-of-plane easy axis, whereas occupation of the d_{z^2} orbital ($l_z = 0$) leads to an in-plane easy axis. The resonance in the hybridization function of the in-plane d orbitals at -2 eV [Figs. 3(e) and 3(f)] indicates a resonance of the Bi_2Se_3 host at this energy which strongly couples to the Fe d_{xy} and $d_{x^2-y^2}$ orbitals. As a consequence, these Fe orbitals are pushed upwards within the energy region -2 eV $\lesssim E \lesssim 0$ eV [cf. Figs. 3(c) and 3(d)] due to level repulsion between the resonance of the Bi_2Se_3 host and the Fe d_{xy} and $d_{x^2-y^2}$ orbitals. Therefore, the Fe d_{xy} and $d_{x^2-y^2}$ orbitals become depopulated, which facilitates in-plane orbital momenta and an in-plane magnetic easy axis [27].

The crystal fields obtained from fitting the spectra of CF multiplet calculations to the XAS or XMCD experiments were $\epsilon_0 = -0.69$ eV and $\epsilon_2 = 0.32$ eV. These values agree qualitatively with the dynamical crystal fields concerning the emptied orbitals, as seen by the solid red curves at energies between $E = -2$ and -1 eV in Figs. 3(c) and 3(d). The fitted experimental spectra are thus in line with the picture that dynamic hybridization effects lead to a depopulation of the Fe d_{xy} and $d_{x^2-y^2}$ orbitals and result in an in-plane magnetic easy axis.

In summary, utilizing a combination of experiment and theory, we demonstrate that the favorable orientation of the magnetic moment of Fe impurities absorbed on the Bi_2Se_3 surface is in-plane with a considerable anisotropy but shows no hysteretic behavior, i.e., magnetic ordering. Furthermore, we show that the favorable orientation of the Fe moment can be well-understood from the interplay between the local atomic physics of the Fe atoms with dynamic hybridization effects induced by the substrate. This illustrates the necessity to account for both local Coulomb interaction and dynamical hybridization effects when considering *ab initio* approaches to address magnetism in these systems. These findings have important consequences for the stability of the TSS of Bi_2Se_3 against perturbations by magnetic Fe impurities, which break time-reversal symmetry. On average, the exchange field by the Fe impurities acts like an in-plane oriented magnetic field $\vec{B}$ on the spins of the surface-state Dirac fermions: $H_D = v_f(\vec{\sigma} \cdot \vec{p}) + g\mu_B \vec{B} \cdot \vec{\sigma}$ [29]. From this Dirac Hamiltonian, it becomes immediately clear that an in-plane exchange field $\vec{B}$, on average, merely shifts the DP to $\vec{p}_D = -g\mu_B\vec{B}/v_F$. Thus, even in the case of in-plane ferromagnetically aligned Fe moments, there is no opening

of a gap, despite the breaking of time-reversal symmetry. Moreover, in the absence of ferromagnetic order, the exchange interaction with the Fe magnetic moments could either lead to random mass terms or random gauge fields acting on the surface-state Dirac fermions. Our finding of an in-plane easy axis shows that the latter type of disorder is preferably realized. The prediction of no gap opening at the DP qualitatively agrees with more recent ARPES results which do not reveal a gap at the DP [9] as previously observed [7]. Furthermore, it has been shown that adsorption of numerous species [10,30,31] leads to similar ARPES spectra, as in Ref. [7]. Resultant valence band quantization after charge transfer [10] exhibits spectral features resembling a gap around the DP, like that originally seen in [7]. Our present finding of an in-plane orientation of the Fe magnetic moments is consistent with the spectral features in question being derived from such a quantization, not a result of broken time-reversal symmetry.

---

*j.honolka@fkf.mpg.de
†Corresponding author.
akhajeto@physnet.uni-hamburg.de

[1] M. Z. Hasan and C. L. Kane, Rev. Mod. Phys. **82**, 3045 (2010).
[2] L. Fu and C. L. Kane, Phys. Rev. Lett. **102**, 216403 (2009).
[3] X.-L. Qi, T. L. Hughes, and S.-C. Zhang, Phys. Rev. B **78**, 195424 (2008).
[4] R. Yu, W. Zhang, H.-J. Zhang, S.-C. Zhang, X. Dai, and Z. Fang, Science **329**, 61 (2010).
[5] Y. S. Hor et al., Phys. Rev. B **81**, 195203 (2010).
[6] Y. L. Chen et al., Science **329**, 659 (2010).
[7] L. A. Wray, S.-Y. Xu, Y. Xia, D. Hsieh, A. V. Fedorov, Y. S. Hor, R. J. Cava, A. Bansil, H. Lin, and M. Z. Hasan, Nature Phys. **7**, 32 (2011).
[8] R. R. Biswas and A. V. Balatsky, Phys. Rev. B **81**, 233405 (2010).
[9] M. Scholz, J. Sanchez-Barriga, D. Marchenko, A. Varykhalov, A. Volykhov, L. Yashina, and O. Rader, preceding Letter, Phys. Rev. Lett. **108**, 256810 (2012).
[10] M. Bianchi, D. Guan, S. Bao, J. Mi, B. B. Iversen, P. D. King, and P. Hofmann, Nature Commun. **1**, 128 (2010).
[11] M. Ye, S. V. Eremeev, K. Kuroda, E. E. Krasovskii, E. V. Chulkov, Y. Takeda, Y. Saitoh, K. Okamoto, S. Y. Zhu, K. Miyamoto, M. Arita, M. Nakatake, T. Okuda, Y. Ueda, K. Shimada, H. Namatame, M. Taniguchi, A. Kimura, and A. Kimura, arXiv:1112.3206.
[12] J. Honolka et al., Phys. Rev. B **76**, 144412 (2007).
[13] J. Wiebe, A. Wachowiak, F. Meier, D. Haude, T. Foster, M. Morgenstern, and R. Wiesendanger, Rev. Sci. Instrum. **75**, 4871 (2004).
[14] A. A. Khajetoorians, S. Lounis, B. Chilian, A. T. Costa, L. Zhou, D. L. Mills, J. Wiebe, and R. Wiesendanger, Phys. Rev. Lett. **106**, 037205 (2011).
[15] T. Hanaguri, K. Igarashi, M. Kawamura, H. Takagi, and T. Sasagawa, Phys. Rev. B **82**, 081305 (2010).
[16] P. Cheng et al., Phys. Rev. Lett. **105**, 076801 (2010).
[17] S. Urazhdin, D. Bilc, S. H. Tessmer, S. D. Mahanti, T. Kyratsi, and M. G. Kanatzidis, Phys. Rev. B **66**, 161306 (2002).
[18] Z. Alpichshev, R. Biswas, A. V. Balatsky, J. G. Analytis, J.-H. Chu, I. R. Fisher, and A. Kapitulnik, arXiv:1108.0022.
[19] S. Stepanow, A. Mugarza, G. Ceballos, P. Moras, J. C. Cezar, C. Carbone, and P. Gambardella, Phys. Rev. B **82**, 014405 (2010).
[20] B. Amadon, F. Lechermann, A. Georges, F. Jollet, T. O. Wehling, and A. I. Lichtenstein, Phys. Rev. B **77**, 205112 (2008).
[21] M. Karolak, T. O. Wehling, F. Lechermann, and A. I. Lichtenstein, J. Phys. Condens. Matter **23**, 085601 (2011).
[22] Here, we employ 6 quintuple layers thick 2×2 Bi_2Se_3 surface supercells containing one Fe adatom and we use the Vienna ab initio simulation package (VASP) [23] with the generalized gradient approximation [24] to the exchange correlation potential and the projector-augmented wave [25,26] basis sets to solve the resulting Kohn-Sham system. We relaxed the positions of the Fe atoms and of the atoms in the uppermost Bi_2Se_3 quintuple layer until the forces were below 0.02 eV $Å^{-1}$.
[23] G. Kresse and J. Hafner, J. Phys. Condens. Matter **6**, 8245 (1994).
[24] J. P. Perdew, K. Burke, and M. Ernzerhof, Phys. Rev. Lett. **77**, 3865 (1996).
[25] P. E. Blöchl, Phys. Rev. B **50**, 17 953 (1994).
[26] G. Kresse and D. Joubert, Phys. Rev. B **59**, 1758 (1999).
[27] See Supplemental Material at http://link.aps.org/supplemental/10.1103/PhysRevLett.108.256811 for a discussion in terms of an Anderson impurity model.
[28] S. Gardonio, T. O. Wehling, L. Petaccia, S. Lizzit, P. Vilmercati, A. Goldoni, M. Karolak, A. I. Lichtenstein, and C. Carbone, Phys. Rev. Lett. **107**, 026801 (2011).
[29] Here, v_f is the Fermi velocity, g the effective Landé factor of the surface-state electrons, $\vec{\sigma}$ are Pauli matrices acting on the spin of the surface-state electrons, and $\vec{p}$ is their momentum.
[30] H. M. Benia, C. Lin, K. Kern, and C. R. Ast, Phys. Rev. Lett. **107**, 177602 (2011).
[31] Z.-H. Pan, E. R. Gardner, S. Cu, Y. S. Lee, and T. Valla, Phys. Rev. Lett. **108**, 117601 (2012).